stellarator news

Published by Fusion Energy Division, Oak Ridge National Laboratory
Building 9201-2 P.O. Box 2009 Oak Ridge, TN 37831-8071, USA

Editor: James A. Rome Issue 54 November 1997
E-Mail: jar@ornl.gov Phone (423) 574-1306 Fax: (423) 241-6211
On the Web at *http://www.ornl.gov/fed/stelnews*

Completion of the LHD poloidal coils and cryostat vessel

Poloidal coils

The largest poloidal coils for the Large Helical Device (LHD), the outer vertical coils, were completed in September 1996. At that time, installation of all poloidal coils began. Important points in the installation are reliable support and high positional accuracy because LHD requires a high-precision magnetic field.

For the poloidal coils, integration of all positional errors was controlled to < 2 mm. Figure 1 shows top and cross-sectional views of the installation structure for the upper inner vertical coil. The coil was partially covered with ten

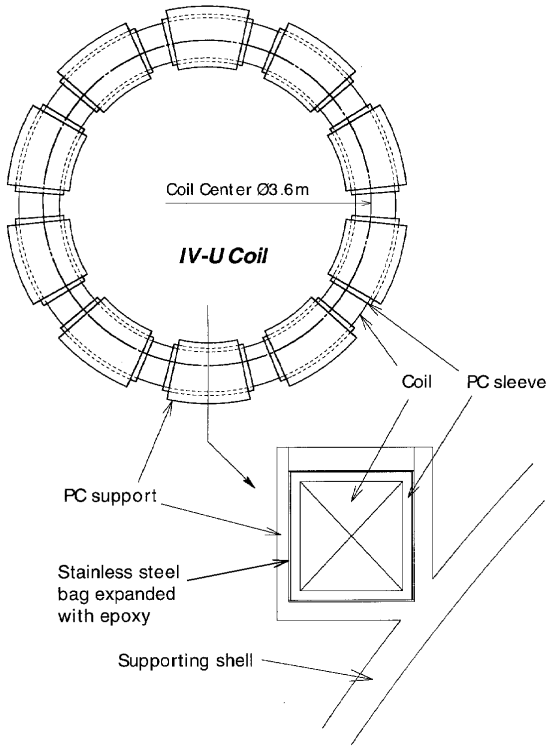

Fig. 1. Top and cross-sectional views of an installed poloidal coil (the upper inner vertical coil).

In this issue . . .

40-mm-thick, fan-shaped stainless steel planks. These planks are called “poloidal coil (PC) sleeves” and contain the supercritical helium. Their roles are to fix the coil to the supporting shell of the LHD and to maintain the coil temperature once the coils are cooled. Positioning lines to indicate the coil center were marked on the upper, inner, and outer surfaces of the PC sleeves.

After inserting the coil with the PC sleeves into the U-shaped “PC supports,” which are fixed to the supporting shell, the coil position was adjusted. The error between the positioning lines on the PC sleeves and PC supports was limited to less than 0.5 mm. Figure 2 shows the upper outer vertical coil being inserted into the PC supports. Special bags made of thin stainless steel plates were inserted between the PC sleeves and supports. After the cover of the PC support was welded in place, the bags were filled with epoxy resin containing glass particles to enhance its mechanical strength. The bags, which expanded and hardened at room temperature, thus fixed the coil position.

Finally, the coil position was checked again. The next step is to install the feeders, piping, and sensors. A superconducting joint is used to connect the feeders to the coil; it is similar to the joint between the double pancakes that make up the coil. The error field due to the feeders is also minimized.

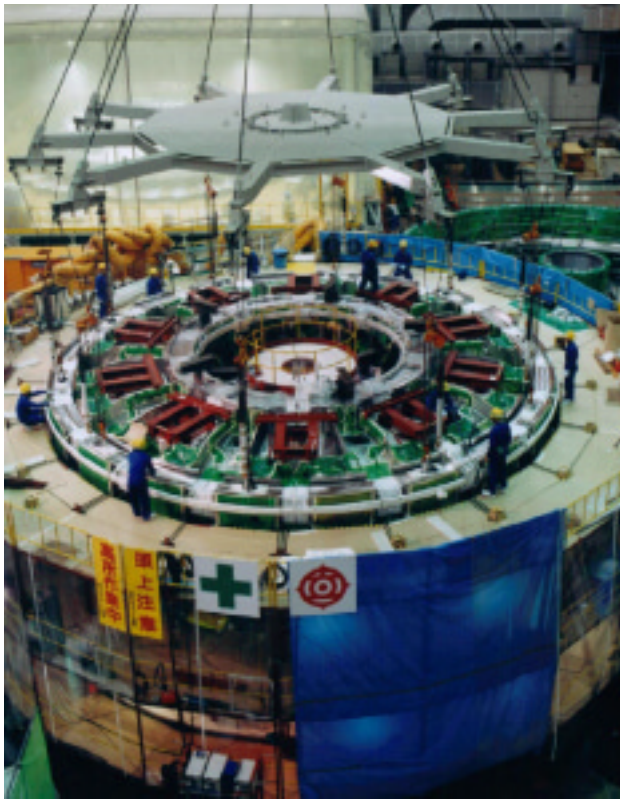

Fig. 2. Installation of the upper outer vertical coil.

Cryostat vessel

The cryostat vessel was moved to its final position at the end of October 1997, marking completion of the construction of the large components of LHD. Work on peripherals around the LHD main device has been started; these include valve boxes for cooling control, a vacuum pumping system, an electron cyclotron heating system, etc.

An adiabatic condition for the LHD superconducting coils and the supporting structure is maintained by the cryostat vessel which is 13 m in diameter and 6.7 m high. This vessel is made of 50-mm and 100-mm-thick SUS304 plates. The radiation shield, which is kept at 80 K, is attached to the inside surface of the vessel. The cryostat vessel consists of four parts: the base, the outer cylinder, the inner cylinder, and the upper cover. The vessel, a torus with a bell-shaped cross section, was designed to surround the inner LHD components and to minimize the deformation generated by atmospheric pressure. The radiation shield is made of SUS316 in thin plates. A coolant pipe is attached on its surface. Thermal insulation, called multilayer insulation (MLI), covers the outside surface of the radiation shield (i.e., between the radiation shielding plate and the inside surface of the cryostat vessel).

The base was assembled at the beginning of the LHD construction, and major LHD components such as the superconducting coils, the supporting structure, and the vacuum vessel were set on the base. The remaining parts of the cryostat vessel were assembled individually and then connected before they were moved into final position. Figure 3 shows the installation of this assembly. The weight of the upper part of the vessel is 180 tons; the total weight, including the hooking jig and wires, is 240 tons. The vessel was lifted by a crane with a capacity of 250 tons. The installation was successfully completed. The upper and the lower part were connected by mechanical joints, and the inside surface of the joint area was welded to be airtight. It is important to ensure high accuracy around the ports on the cryostat, which will be used for plasma heating or diagnostics. The estimated final accuracy in these areas is within 5 mm.

Kazuya Takahata and Hitoshi Tamura for the LHD team
National Institute for Fusion Science
322-6 Oroshi-cho, Toki-shi, Gifu 509-52, Japan
E-mail: takahata@LHD.nifs.ac.jp / tamura@LHD.nifs.ac.jp

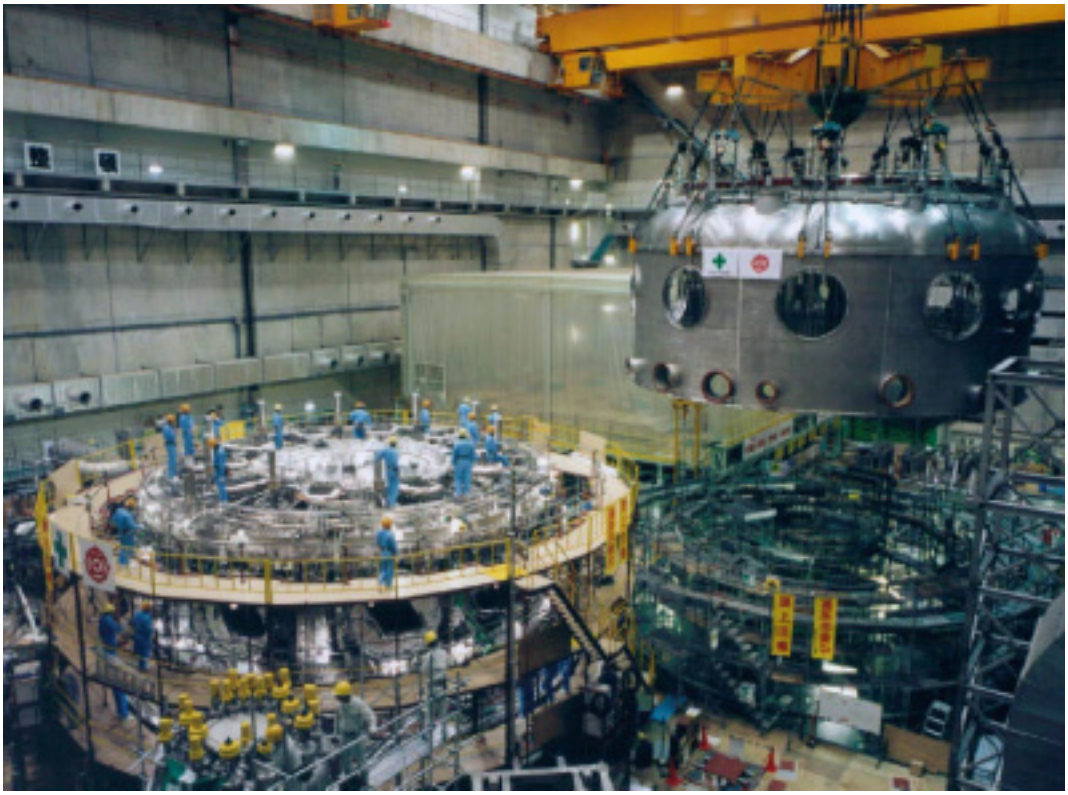

Fig. 3. Moving of the cryostat vessel to the final position.

Optimum confinement discharges at W7-AS

Introduction

High temperatures are most important for the transport (lmfp) regime. In the lmfp regime, neoclassical theory predicts an unfavorable dependence of the transport coefficients on temperature. Thus, transport analysis in low-collisionality plasmas is best suited for the examination of neoclassical predictions. Neoclassical theory seems to be a fairly reliable tool which may be used in predictive transport codes to examine the performance of future large stellarators.

Close to the plasma edge at low temperatures, neoclassical theory fails. Confinement in this region is dominated by anomalous transport (i.e., the physics is not yet understood). Especially in Wendelstein 7-AS (W7-AS), which has fairly low vacuum shear, the confinement properties depend sensitively both on the value of the rotational transform ι (low-order rational values of ι can lead to confinement degradation) and on its shear. The shear in the **E** $\times$ **B** rotation may also play a role in confinement. Here we concentrate on the confinement properties in the bulk plasma for optimum conditions.

Experimental Details and Interpretation

We examine three types of neutral beam injection (NBI) heated discharges in W7-AS with optimum confinement properties which exceed the ISS95 scaling [1] by at least a factor of 2.

In purely NBI-heated discharges with a power of $P_{\mathrm{NBI}} \leq$ 400 kW, a maximum value of $\tau_E \approx 50$ ms has been determined. In the upper part of Fig. 1 the development of various discharge parameters is shown. During the transition to good confinement, the density profile becomes narrow, whereas the temperature profile broadens. In both profiles, the gradients steepen and the radial electric field E_{r} decreases in the gradient region to $E_{\mathrm{r}} \leq -180$ V/cm. Both density and temperature show very low values at the edge (Fig. 1, lower part), which is contrary to NBI discharges in the "early phase" of W7-AS operation. In high-power discharges with NBI and electron cyclotron resonance heating (ECRH), shown in Figs. 2 and 3 for medium and high density, a narrow density profile allows steep temperature gradients (and large $E_{\mathrm{r}} < 0$) close to the plasma edge where n_{e} becomes very small. For these types of discharges, optimum confinement properties are found ($T_{\mathrm{e}} > T_{\mathrm{i}} \approx 1.5$ keV at medium density). The experimental particle fluxes as well as the ion and electron energy fluxes are in good agreement with the neoclassical predictions up to 70% of

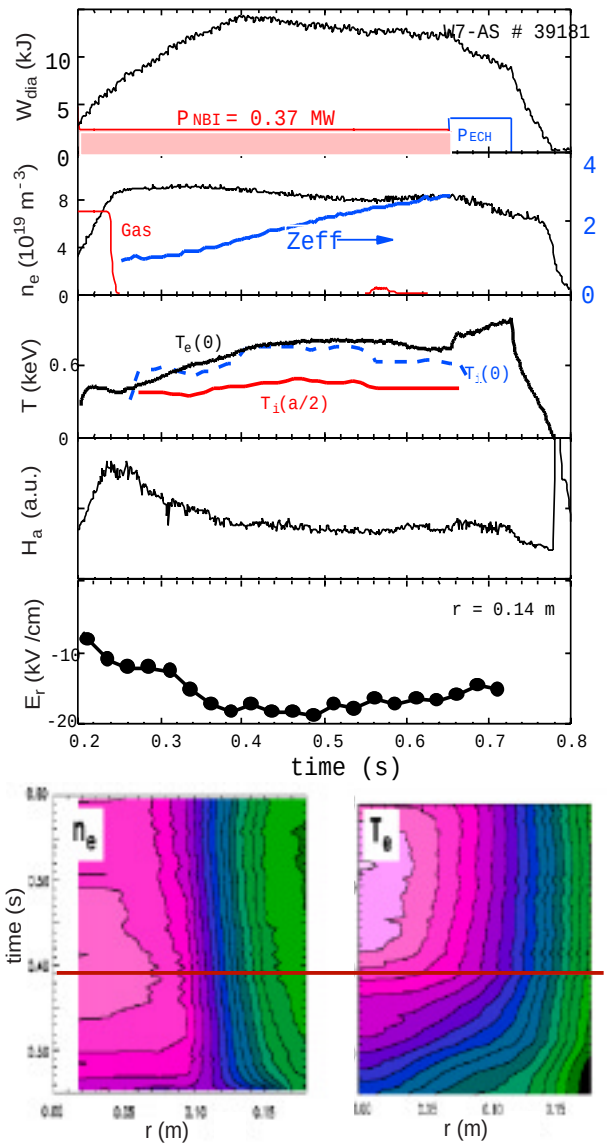

Fig. 1. Top part: Time sequences of various experimental quantities during discharge 39181 with maximum $\tau_E \approx 50$ ms. Bottom part: Density and electron temperature contours of the same discharge. The line indicates the time of energy analysis.

the plasma radius; see Ref. [2]. Furthermore, the predicted E_r obtained from the ambipolarity condition of the neoclassical fluxes is also consistent with the experimental findings [3] at the outer radii, where the ambipolar neoclassical fluxes become very small. These findings indicate that the additional anomalous particle fluxes may be intrinsically ambipolar.

Good wall conditioning and very low recycling are mandatory to obtain the required narrow density profiles and to provide global density control even for high NBI power levels (with a particle source strength of up to 2.5×10^{20} s^{-1}). Moreover, the outer density profile is (within the experimental errors) independent of both the central density and the heating power [4]. Here, the T_e gradient at the outer radii reflects the heating power. Furthermore, $T_e \approx T_i$ is found in this region [3]. The steep temperature gradients flatten in the bulk region because of the strong temperature dependence of the neoclassical transport coefficients, leading to the optimum confinement in this type of discharges.

Neoclassical calculations [4] using the DKES code are in good agreement with the experimental transport analyses in low-collisionality W7-AS plasmas, i.e., in the bulk plasma at sufficiently high temperatures. This holds for the ion and electron heat conduction as well as for the particle transport. The predicted ambipolar electric field is also consistent with experimental findings, except for those radial positions where very large values of E_r are observed. In neoclassical theory, electric fields are basically assumed to be small.

The common feature of the three discharge types discussed above is that τ_E exceeds the ISS95 scaling by about a factor of 2. A maximum value of $\tau_E \sim 50$ ms has been obtained so far, see Fig. 4.

M. Kick and H. Maaßberg for the W7-AS, ECRH and NBI Teams
IPP Garching, Germany (EURATOM-Association)
E-Mail: kick@ipp-garching.mpg.de

References

[1] U. Stroth et al., Nucl. Fusion **36**, 1063 (1996).

[2] R. Jaenicke et al., Plasma Phys. Controlled. Fusion **37**, A163 (1995);
M. Kick et al., paper F1-CN-64/C1-4 presented at the 16th IAEA Conf. Plasma Phys. Controlled Nucl. Fusion Res., 1996.
F. Wagner, M. Kick and W7-AS Team, presented at the 11th International Stellarator Conference & 8th International Toki Conference, 1997 (proceedings to be published).

[3] J. Baldzuhn et al., presented at the 11th International Stellarator Conference & 8th International Toki Conference, 1997 (proceedings to be published).

[4] H. Maaßberg et al., presented at the 11th International Stellarator Conference & 8th International Toki Conference, 1997 (proceedings to be published).

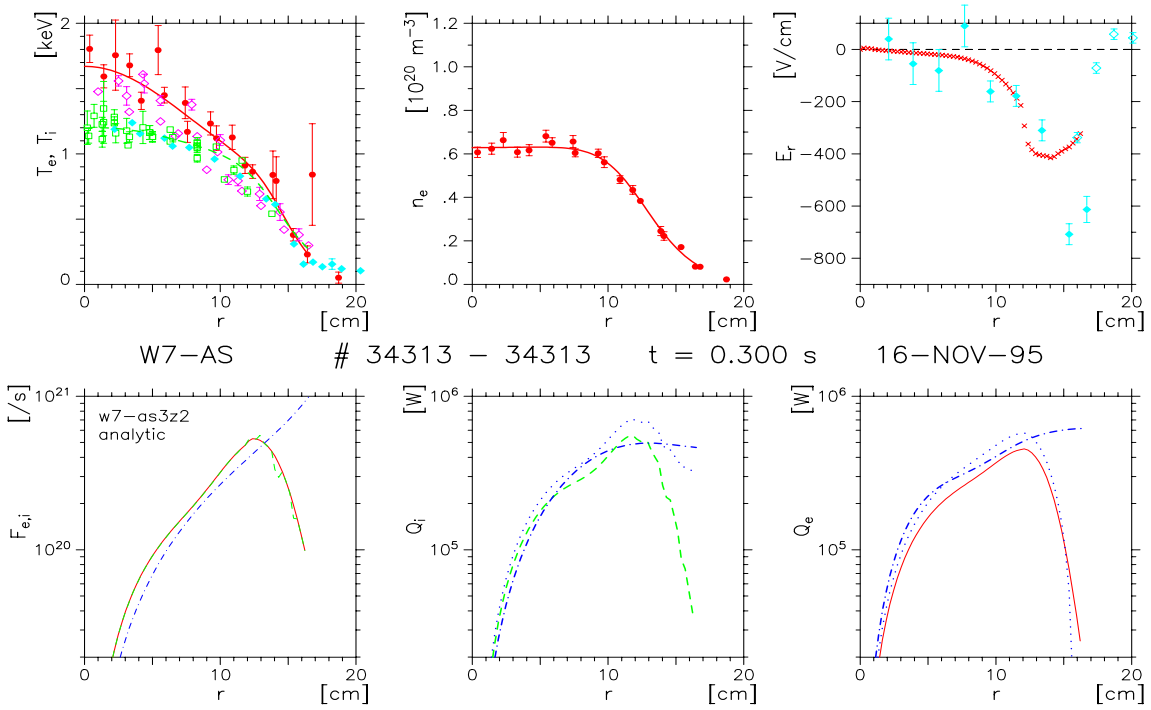

Fig. 2. Optimum confinement at medium density, discharge 34313, combined ECRH and NBI, $P_{ECRH} \approx 750$ kW, $P_{NBI}^{abs} \approx 900$ kW. In the upper-left part, T_e (dark symbols) from Thomson scattering (red) and ECE (magenta) and T_i (light symbols) from active CX-NPA (green) and CXRS (cyan); n_e from Thomson scattering (upper middle), radial electric field (upper right, cyan) as deduced from active CXRS (dots) and passive spectroscopy (circles) compared to the neoclassically calculated ambipolar electric field (red crosses). In the lower part, the experimental particle $F_{e,i}$ and energy fluxes $Q_{i,e}$ for ions and electrons, respectively, are compared with neoclassical predictions by DKES code for ions (green) and electrons (red) , taking the ambipolar electric field (upper right) into account.

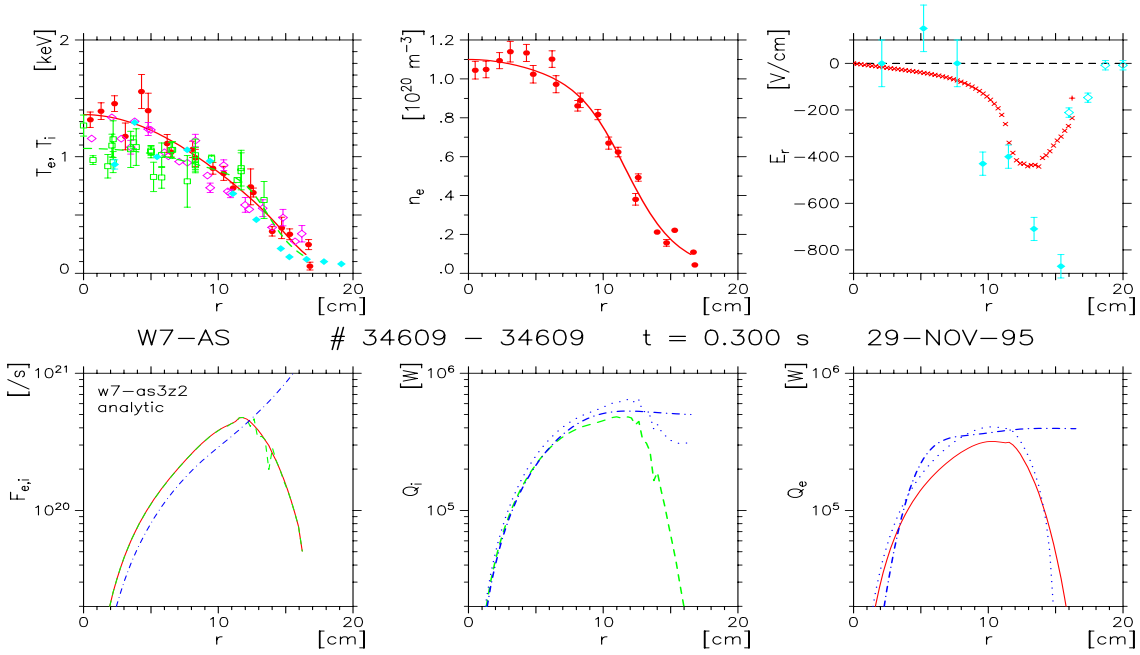

Fig. 3. Optimum confinement at high density, discharge 34609, combined ECRH and NBI, $P_{ECRH} \approx 350$ kW, $P_{NBI}^{abs} \approx$ 900 kW. The symbols are as in Fig. 2.

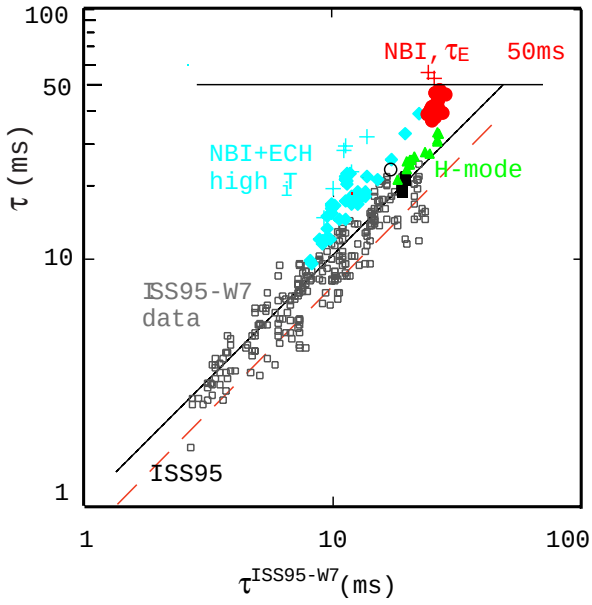

Fig. 4. Energy confinement times in W7-AS compared to ISS95-W7. Dashed line: ISS95 for all helical devices; solid line: ISS95-W7 for W7-AS data up to 1995. Open squares: pure ECRH; solid triangles: ECRH H-mode; solid circles: low power NBI, leading to $\tau_E \approx 50$ ms, open circles: NBI with higher power; full (light) diamonds: combined NBI and ECRH, leading to $T_i \approx 1.5$ keV. Crosses for the same discharges indicate the effects of taking the kinetic instead of the diamagnetic energy. Both sets of data with NBI, circles and diamonds, show the increase of τ_E by about a factor of 2.

Compact stellarator configurations with Helical Post

Stellarators are normally large-aspect-ratio devices (aspect ratio, A, is the ratio of the average major radius to the average minor radius for the last closed flux surface), with A usually 7–10 (see, for example, Refs. [1–4]). The lowest-A stellarators ever built have A ~ 5 [5–7].

Recently, the Spherical Stellarator (SS) concept [8–9], called so in analogy with the Spherical Tokamak (ST) concept [10–11], was proposed. The main characteristics of a SS are: (a) very low plasma aspect ratio, $A \leq 3.5$, (b) high β limits, well above the 3–5% typical for traditional stellarators, and (c) positive, strong plasma current. Here, positive means that the current flows in such a direction that the total rotational transform increases in comparison with its vacuum value, and strong means that its contribution to the total rotational transform is significant. In a large and high-β SS, the required plasma current can be fully supported by the bootstrap effect [9, 12] and thus does not require any current drive technique. Goals of the SS approach include improved particle transport and simplicity of the coils. An SS with somewhat similar characteristics was mentioned in Ref. [13]. For small SS devices which cannot rely on significant bootstrap current, the ohmic or auxiliary driven current can be used in the corresponding experiments.

A few SS configurations, differing principally in the types of simple coils to be used, have been analyzed [8–9, 12–16]. Coil configurations with a straight center post, planar coils, and outboard stellarator windings have been considered. More complicated coils combining a few different types are possible as well. Researchers at ORNL are investigating a closely related concept, the SMARTH (SMall Aspect Ratio Toroidal Hybrid) [12, 17–20]. Some other U.S. institutions including PPPL [21] have also become involved in this kind of low-aspect-ratio stellarator research.

We propose a novel class of stellarators with a few very unique and advantageous characteristics, not only in comparison with the traditional large-aspect-ratio stellarators but also in comparison with the SS configurations considered so far. These Helical Post Stellarators (HPS) have: (a) extremely low plasma aspect ratio, $A \leq 1.4$, (b) a simple coil system featuring a helical center post, (c) extremely high β limits assisted by a strong positive bootstrap current, and (d) improved particle transport characteristics. The helical post can be a single helix or may consist of a few helices.

Here we briefly introduce the HPS configurations and demonstrate their advantages. We present a few results for a single-helix stellarator (SHS), a double-helix stellarator (DHS), and a triple-helix stellarator (THS). In the configurations considered, the helical center post is the only helical element of the coil system responsible for the stellarator characteristics. More complicated configurations combining the helical center post with the other helical elements of the coil system are possible but are beyond the scope of this paper.

To our knowledge, the HPS configurations considered are unique among all previously considered stellarators, including the SS analyzed so far, in that the magnetic field ripple is located practically entirely on the inboard of the torus. This improves particle transport, according to theory [22–23].

The coil systems of the HPS configurations considered are shown in Fig. 1. The outboard parts of the toroidal field (TF) coils and the system of the poloidal field (PF) rings are the same as in a typical ST. The difference, however, is in the helical center post, and the three cases presented correspond to (a) SHS, (b) DHS, and (c) THS. The top views of the last closed vacuum flux surface for these three con-

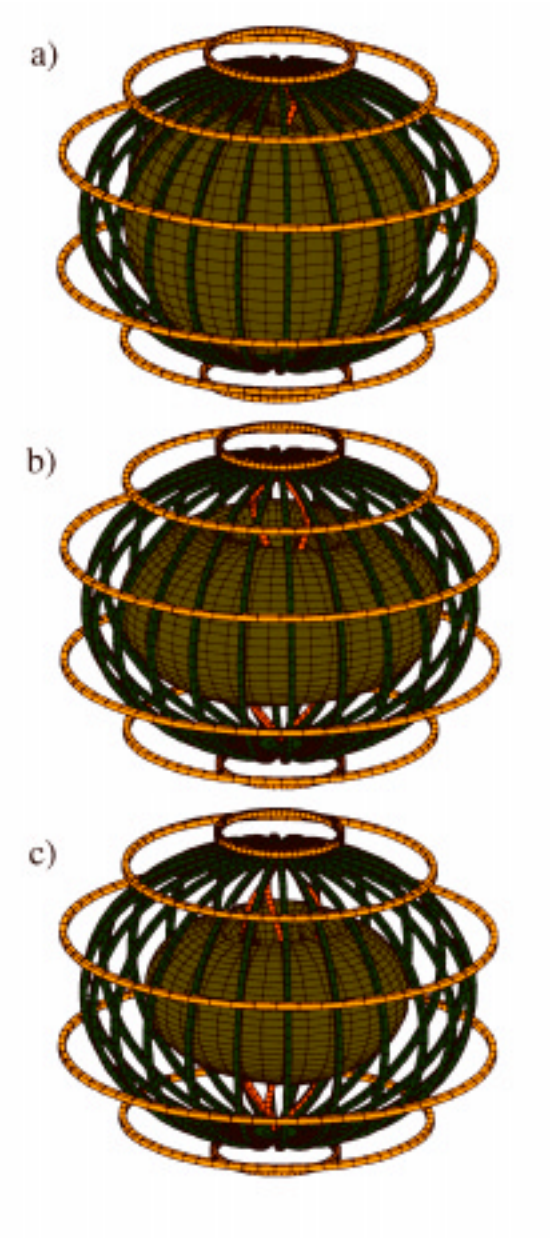

Fig. 1. The coil systems and LCFS of (a) SHS, (b) DHS, and (c) THS.

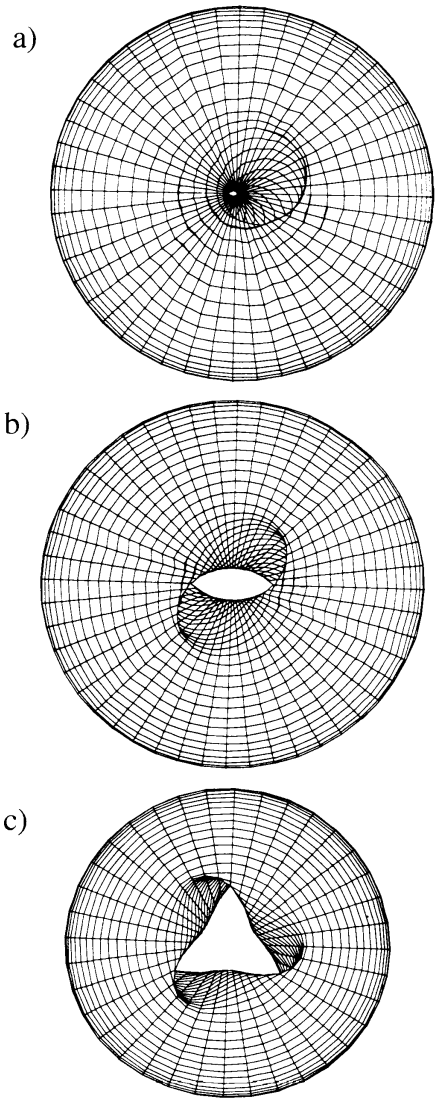

Fig. 2. Top view on the last closed vacuum flux surface in (a) SHS, (b) DHS, and (c) THS.

figurations are shown in Fig. 2. The PF rings are actually used in these calculations only for an SHS to push the plasma further inside to reduce the magnetic ripple. Generally, the vacuum flux surfaces with large enclosed volumes and significant rotational transform can be obtained without PF rings for all HPS configurations considered. However, the PF rings are necessary for obtaining high-β MHD equilibria.

The HPS configurations feature extremely low aspect ratios: $A \sim 1$ for the SHS, $A \sim 1.1$ for the DHS, and $A \sim 1.2$ for the THS. To our knowledge, the SHS is the first stellarator configuration ever considered that has only a single toroidal period.

To further demonstrate the general advantages of the HPS concept, we present here a few results of calculations with the three-dimensional (3-D) MHD equilibrium code VMEC [24], running in free-boundary mode, the 3-D field line tracing code UBFIELD [25], and the 3-D bootstrap current code BOOTSJ [26, 9]. Much more detailed analysis will be given in separate publications [27, 28].

A typical radial profile of the vacuum rotational transform for an HPS is shown in Fig. 3.

To demonstrate the improved particle transport characteris-

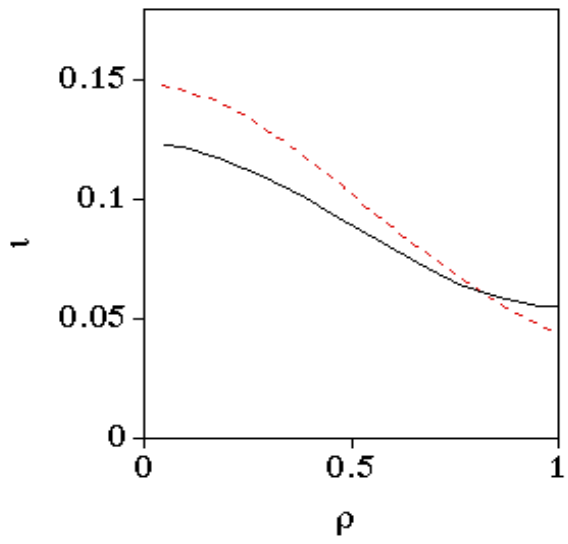

Fig. 3. Radial dependence of the rotational transform for the SHS without PF rings (solid curve) and with PF rings (dashed curve).

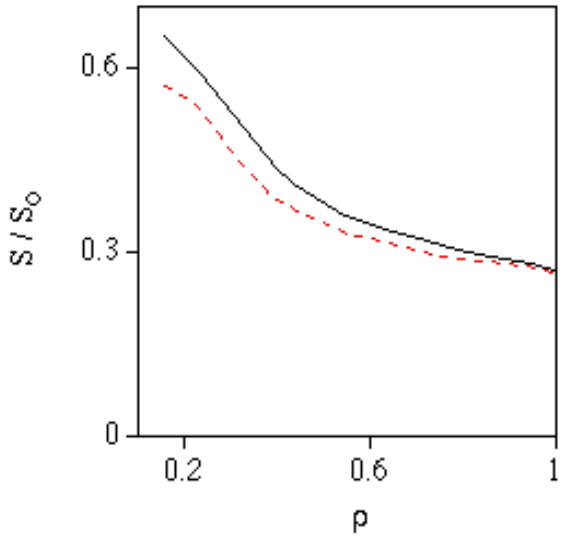

Fig. 4. Radial dependence of S/S_0 for the SHS without PF rings (solid curve) and with PF rings (dashed curve).

tics in the HPS, Fig. 4 shows the ratio S/S_0 for the SHS configurations in Fig. 3. Here, the parameter S [23] is proportional to the neoclassical flux, and S_0 corresponds to the nonoptimized stellarator case when the helical ripple is distributed evenly on each flux surface. Improvement by a factor of 2 to 3, depending on minor radius, is clearly seen.

A typical |**B**| distribution along flux surfaces of an HPS is shown in Fig. 5, where the case of vacuum DHS field is presented and the last flux surface is considered. All HPS configurations considered have a common feature in |**B**| distribution: quasi-helical symmetry on the inboard side of the torus and quasi-toroidal symmetry on the outboard side.

To demonstrate the extremely high β characteristics of the HPS, the left column of Fig. 6 shows the flux surfaces for the MHD plasma equilibrium in a DHS at the central β_0 = 86% and the volume average β = 20%. This equilibrium corresponds to a toroidal flux $\Phi \sim 0.2$ Wb, self-consistent bootstrap current $I_{bs} \sim 300$ kA, and the total rotational transform increasing from about $\iota \sim 0.15$ near the magnetic axis to $\iota \sim 0.3$ at the plasma boundary. Here, $\iota = 1/q$, with q the safety factor. Such an increase of ι with minor radius at high β might be advantageous for suppression of magnetic islands [29]. The contours of |**B**| for the same three main cross sections are shown in the right column of Fig. 6. The partial omnigeneity [30] (for the ideal case, the |**B**| contours coincide with the flux surfaces) is clear. This is advantageous for further improvement of particle transport in the HPS. Location of the minimum |**B**| near the magnetic axis in all cross sections causes the radial β profile to be much more peaked than the corresponding pressure profile.

In conclusion, a new class of stellarators, the HPS, was introduced and particular examples for the SHS, DHS, and THS configurations were presented. Many unique characteristics such as extremely low aspect ratio, extremely high β MHD equilibria, and improved particle transport were demonstrated. The HPS can be built relatively easily by replacing the straight center post of an ST with a helical center post or possibly by winding a helix around the straight center post of an ST. The main goal of such a transformation is to obtain a device with advanced characteristics which can operate in a steady-state regime for any given plasma pressure below some high limit. Further research and optimization are in progress.

Paul E. Moroz
Center for Plasma Theory and Computation
Department of Engineering Physics
University of Wisconsin–Madison
Madison, WI 53706, USA

Phone: (608) 263-7128
E-mail: moroz@engr.wisc.edu

This work was supported by the U.S. Department of Energy, under Grant DE-FG02-97ER54395.

References

[1] J. H. Harris et al., Fusion Technol. **17**, 51 (1990).
[2] J. Sapper et al., Fusion Technol. **17**, 62 (1990).
[3] C. Beidler et al., Fusion Technol. **17**, 148 (1990).

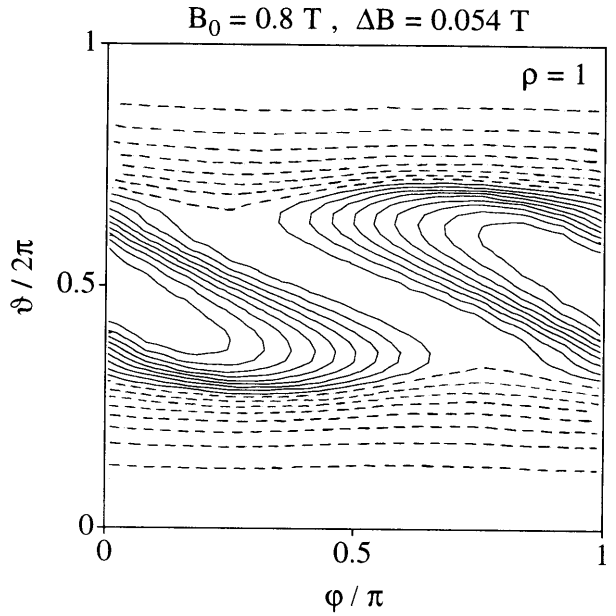

Fig. 5. |**B**| distribution on the last closed vacuum flux surface of the DHS. Solid contours are for $B \geq B_0$, dashed for $B < B_0$; ΔB is the difference between adjacent contours.

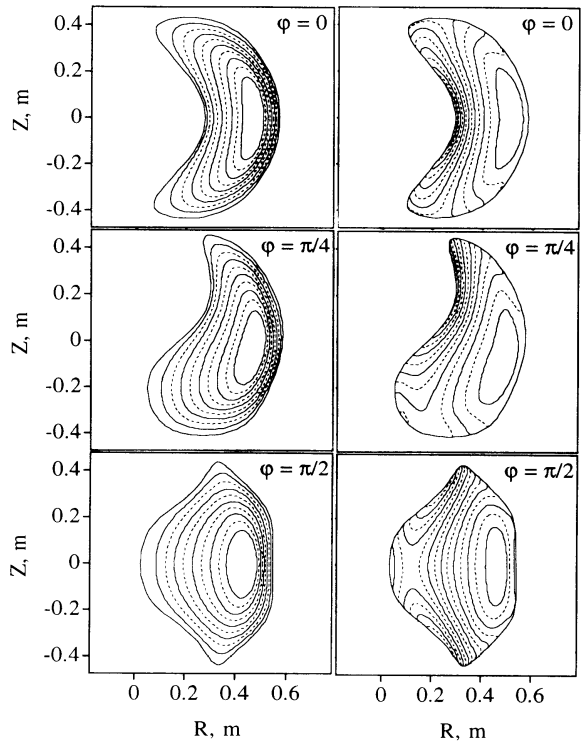

Fig. 6. High-β (β_0 = 86%, β = 20%) MHD equilibrium in the DHS with self-consistent bootstrap current. Left: flux surfaces. Right: contours of |**B**|.

[4] M. Wakatani et al., Plasma Phys. Controlled Fusion **38**, 937 (1996).

[5] K. Nishimura et al., Fusion Technol. **17**, 86 (1990).

[6] M. G. Shats et al., Phys. Rev. Lett. **77**, 4190 (1996).

[7] S. F. Knowlton et al., J. Fusion Energy **12**, 261 (1993).

[8] P. E. Moroz, Phys. Rev. Lett. **77**, 651 (1996).

[9] P. E. Moroz, Phys. Plasmas **3**, 3055 (1996).

[10] M. Peng et al., Nucl. Fusion **26**, 576 (1986).

[11] A. Sykes, Plasma Phys. Controlled Fusion **36**, B93 (1994).

[12] P. E. Moroz et al., Fusion Tech. **30**, 1347 (1996).

[13] P. E. Moroz, Stellarator News **48**, 2 (1996).

[14] P. E. Moroz, Pl. Phys. Controlled Fusion **39**, 1841 (1997).

[15] P. E. Moroz, Plasma Phys. Rep. **23**, 502 (1997).

[16] P. E. Moroz, Nucl. Fusion **37**, 1045 (1997).

[17] [B. A. Carreras et al., Configuration Studies of a Small Aspect Ratio Tokamak-Stellarator Hybrid, ORNL/TM-13252, Oak Ridge National Laboratory (Aug. 1996).

[18] D. A. Spong et al., Plasma Phys. Rep. **23**, 483 (1997).

[19] D. A. Spong et al., *Stellarator News*, No. 52, 1 (1997).

[20] D. W. Ross et al., Plasma Phys. Rep. **23**, 492 (1997).

[21] R. J. Goldston, IAEA Tech. Committee Meeting., Pleasanton (Oct. 1997).

[22] H. E. Mynick et al., Phys. Rev. Lett. **48**, 322 (1982).

[23] K. C. Shaing et al., Phys. Fluids **28**, 2136 (1983).

[24] S. P. Hirshman et al., Comput. Phys. Commun. **43**, 143 (1986).

[25] P. E. Moroz, Phys. Plasmas **2**, 4269 (1995).

[26] K. C. Shaing et al., Phys. Fluids B **1**, 1663 (1989).

[27] P. E. Moroz, Helical Post Stellarator, UW-CPTC 97-15, Univ. Wisconsin, Madison (1997), submitted for publication.

[28] P. E. Moroz, "Double Helix Stellarator," UW-Madison Report UW-CPTC 97-16 (1997), submitted for publication.

[29] R. J. Goldston, paper 2C26 presented at the International Sherwood Fusion Theory Conference, Madison, Wisconsin, April, 1997.

[30] L. S. Hall et al., Phys. Fluids **18**, 552 (1975).

Review of 3-D equilibrium calculations and reconstructions for W7-AS, Part II

Equilibrium recovery using function parametrization

Interpretive methods for determining plasma equilibria from experimental data, such as magnetic measurements, are widely used in tokamak analysis. For tokamaks, input parameters to an equilibrium code are iteratively adjusted such that simulated diagnostic signals from the resulting equilibrium best match experimental data. Since a full solution of the three-dimensional (3-D) equilibrium using the NEMEC [1] code for standard W7-AS conditions requires roughly one hour of CPU time on the Cray J-90, this approach is generally unsuitable for stellarators because each iteration involves at least one equilibrium calculation.

Instead of solving the equilibrium exactly, we apply function parameterization (FP) methods [2] to equilibrium reconstruction on W7-AS. FP seeks simple functional relationships between plasma parameters and diagnostic measurements over a database of calculated equilibria. This facilitates rapid equilibrium reconstruction, here in terms of a prescribed pressure profile (as a function of the normalized toroidal flux) and/or given magnetic data. We have developed a novel interpretive method for equilibrium identification based on FP reconstructions that can be performed in the order of a few tens of seconds on a workstation.

FP database

Our database consists of about 400 net toroidal current-free equilibria calculated with the NEMEC code. Magnetic islands and separatrix structures are not considered since NEMEC assumes nested toroidal flux surfaces. The database equilibria are randomly chosen by varying eight input parameters over ranges appropriate to W7-AS, namely three ratios of the four field-coil currents, the maximum vertical extent of the boundary flux surface in the elliptical ($\phi = 36°$) plane corresponding to the position of the up/down limiters, and a 4-parameter pressure profile chosen from the following family (s is the normalized toroidal flux):

$$p(s) = p_0(1-s)^2\exp(as + bs^2 + cs^3)$$

This admits a wide variety of possible profile shapes in the database, a selection of which is shown in Fig. 1. Some summary statistics for the database, including both input and output parameters are detailed in Table 1. Plasmas with a wide range in both physical size (volume) and beta values are encompassed.

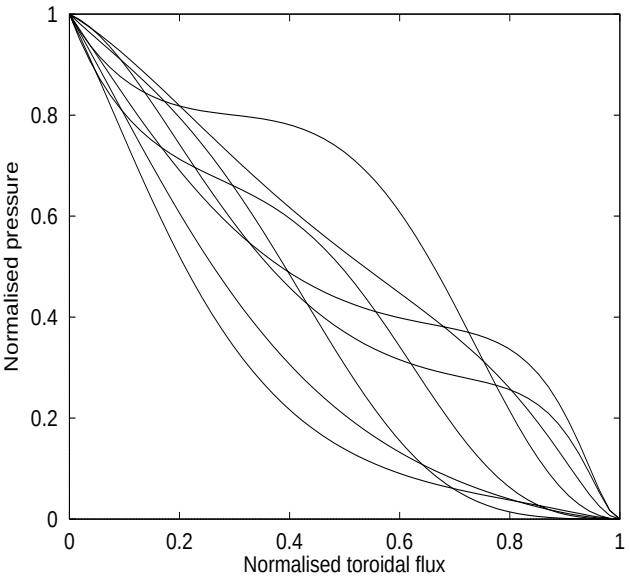

Fig.1. Some equilibrium pressure profile shapes vs normalized toroidal flux p_{eq} (s) in the database.

FP models

Predictors for use in FP models are selected according to twin criteria: they should be independent for good conditioning of the regression problem and they should be as few as possible to keep the model size small. The parameters chosen here fall into two groups: those describing the vacuum magnetic field and those describing the plasma contribution. The former are the three external magnetic coil current ratios and the limiter position (all of which are

Table 1. Database summary statistics

Variable	Mean	Std. Dev.	Minimum	Maximum
I_{mod} (kA)	15.50	0	15.50	15.50
I_{son} (kA)	14.84	4.3	9.69	26.12
I_{tor} (kA)	2.16	5.2	–10.39	10.74
I_{vert} (A)	412.32	245.2	1024.46	7.25
Z_{lim} (m)	0.271	0.033	0.221	0.339
p_0 (kPa)	11.61	5.16	2.03	20.00
a	–0.57	1.60	–4.80	1.97
b	2.88	4.68	–9.19	9.99
c	–1.47	4.88	–9.97	9.61
r_{eff} (cm)	15.3	1.7	11.2	19.5
V (m^3)	0.94	0.21	0.49	1.54
W_{MHD} (kJ)	6.45	3.50	0.73	19.04
ι_{axis}	0.38	0.06	0.25	0.54
ι_{edge}	0.32	0.07	0.16	0.46
β_{axis} (%)	1.89	0.93	0.42	4.50

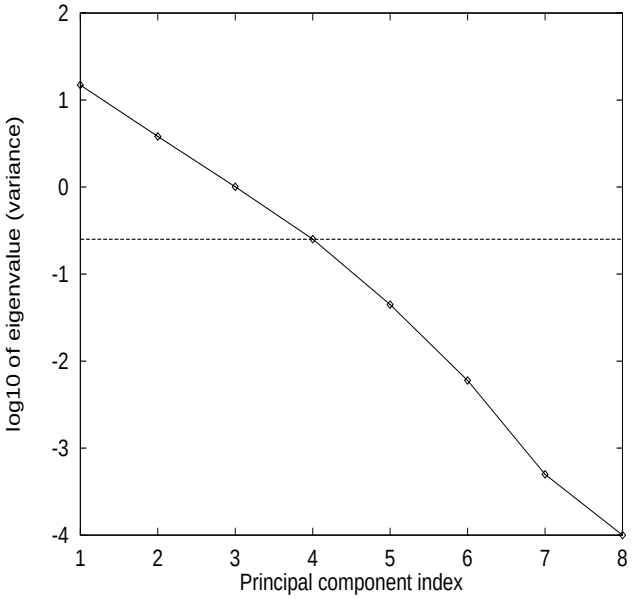

Fig. 2. Log base 10 of principal component eigenvalue (variance) vs PC index for the first few PCs.

independent by design). The latter are constructed by carrying out a principal component (PC) analysis of the equilibrium pressure evaluated at a number of fixed *s* values. The resulting PCs are linear combinations of the pressure data which are uncorrelated over the database. The variance of the PCs decreases with increasing PC index. Figure 2 shows a log plot of variance versus PC index for the first few PC's. Retaining only those with significant variance results in dimension reduction; here we retain the first 4 PC's which account for over 99.7% of the total variance.

Investigation of parameter dependencies over the database reveals that the optimum model for parameter recovery is a second-order one in the above predictors. Profile quantities are modeled by combining this model with a radially varying function, here a polynomial in the square root of the normalized toroidal flux. The 3-D flux surface geometry is recovered by separate modeling of its Fourier coefficients, which is convenient since NEMEC outputs equilibrium flux surfaces and magnetic field in spectrally minimized Fourier form.

Given these conditions, FP equilibrium reconstructions (including global parameters such as W_{MHD}, volume, and 3-D flux surface geometry) can be performed in a few seconds on a workstation, and agree well with those calculated by NEMEC. FP's large speed advantage over conventional methods means that an interpretive procedure based on FP reconstructions is feasible, even if many equilibria must be calculated per iteration.

Interpretive scheme for equilibrium identification

On W7-AS, equilibrium identification based solely on the routinely available magnetic measurements is not possible since these measurements provide only the energy content. Therefore, we have chosen an alternative approach using profile data for this purpose.

The Thomson scattering diagnostic on W7-AS currently gives electron temperature and density (and thus the electron pressure p_e) on up to 20 channels along a horizontal line of sight through the magnetic axis in a symmetry plane ($\phi = 0°$) at a single time point during a discharge, i.e., $p_e = p_e(R_i)$, R_i being the major radii of the Thomson channels. A smoothing polynomial in R is fitted to the p_e data, allowing evaluation between channels.

An iterative procedure attempts to reproduce the spatial to flux transformation assuming p_e is constant on flux surfaces: Starting from an initial guess, the equilibrium pressure profile $p_{eq}(s)$ is varied to minimize the quantity

$$\int \{p_e[R_{in}(s)] - p_e[R_{out}(s)]\}^2 ds$$

subject to the constraint that $p_{eq}(s)$ is not hollow. $R_{in}(s)$ and $R_{out}(s)$ are the high- and low-field radii on the same flux surface taken from the FP recovered equilibrium. The interpreted fit thus depends only on the topology of the $p_e(R)$ profile and not on its magnitude. In fact, it can be done separately for the Thomson temperature and density profiles. An additional restriction—that the kinetic energy content match the diamagnetic energy from the experiment—can be optionally enforced; this lends stability to the procedure when the input data are of poor quality.

However, mismatches between the theoretical and physical magnetic configurations could falsify the present scheme as well as the standard calculations. Consistency checks with additional spatially resolved or global diagnostic data would reveal such discrepancies, if present. This has not yet been done.

Comparison with standard equilibrium calculations

Results from the interpretive method and the standard NEMEC simulation for two experimental shots, one at medium beta (#31119) and one at high beta (#31909) are compared in Figs. 3 and 4. The upper table and two plots in each case show the experiment parameters, the Thomson $p_e(R)$ with smoothing polynomial and the interpreted $p_{eq}(s)$, and the standard NEMEC profile. The lower three plots show the interpreted and standard NEMEC ι profiles, the equilibrium flux surfaces in the Thomson ($\phi = 0°$) plane and the final asymmetry error $\Delta p_e(s)$ (the difference between p_e evaluated at inner and outer R points of equal flux). Solid lines refer to interpreted quantities, and dashed lines indicate those for the standard NEMEC simulation.

In both cases the standard calculation and interpreted fit are comparable in quality, but the interpreted fit produces a lower RMS $\Delta p_e(s)$. This is not unexpected since the standard calculation uses the same optimization criterion with a less flexible pressure profile and with manual intervention

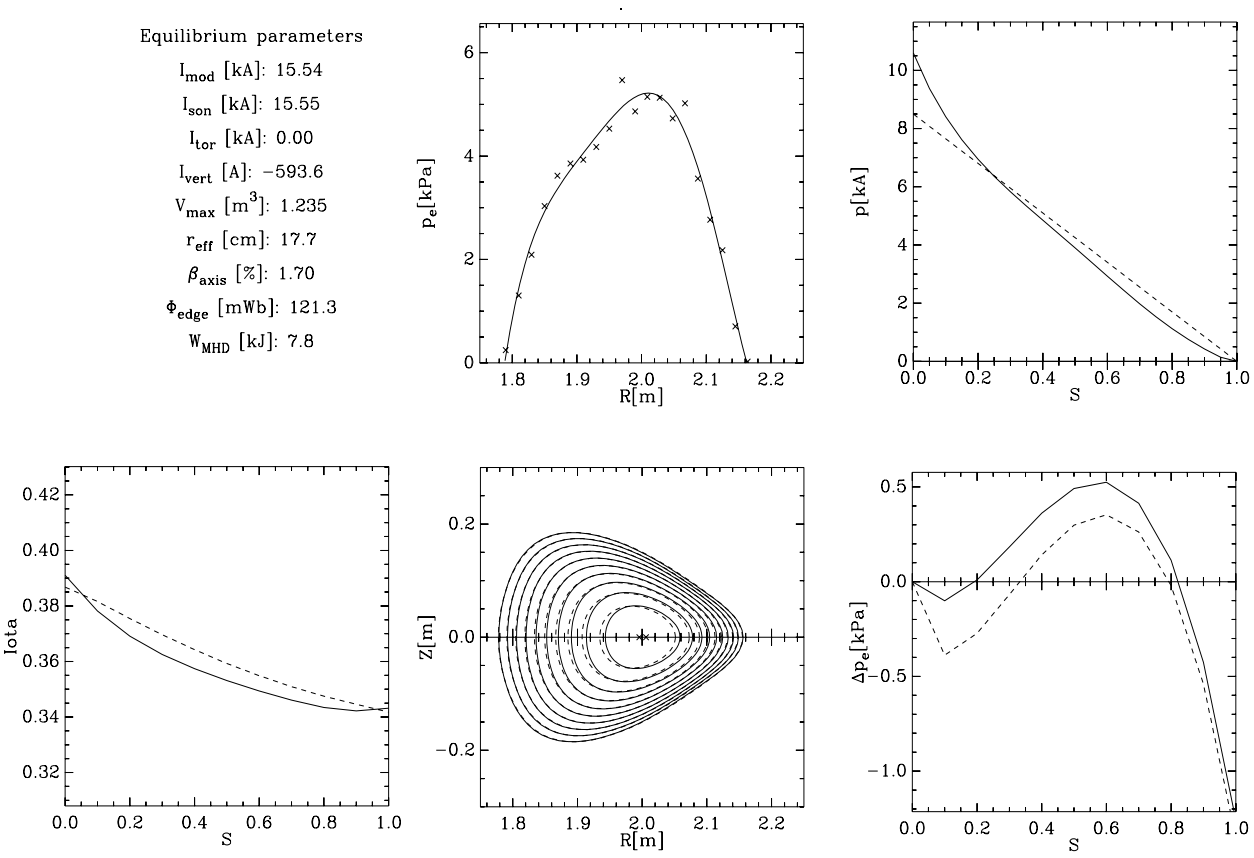

Fig. 3. Comparison of interpreted fit (solid) and standard NEMEC calculation (dashed) for shot #31119 (for further explanation see text).

required between iterations, rather than a least-squares criterion. Δp_e can be further improved by varying additional pressure parameters during iterations; three of a possible four were varied here to prevent overfitting. The interpretation for this case took roughly 20 s on a workstation, which is three orders of magnitudes faster than the standard simulation, which required several NEMEC calculations.

Work in progress includes investigation of the effects of signal noise on the recovery. Moreover, although global equilibrium parameters and flux geometry are well recovered, a model that reproduces the ι profile well has so far proved elusive. Once this is achieved, the procedure will be applied to equilibria with finite net toroidal current.

H. Callaghan, J. Geiger,[a] P. McCarthy
Dept. of Physics, University College Cork
Association Euratom-DCU, Cork, Ireland
[a]Max Planck Institut für Plasmaphysik
D-85748 Garching, Germany
EURATOM Assoziation
E-mail: H.Callaghan@ucc.ie

References

[1] S.P. Hirshman, W. I. van Rij. and P. Merkel, Comput. Phys. Commun. **43,** 163 (1986).

[2] P. J. McCarthy, "An Integrated Data Interpretation System for Tokamak Discharges," Ph.D. thesis, University College Cork, 1992.

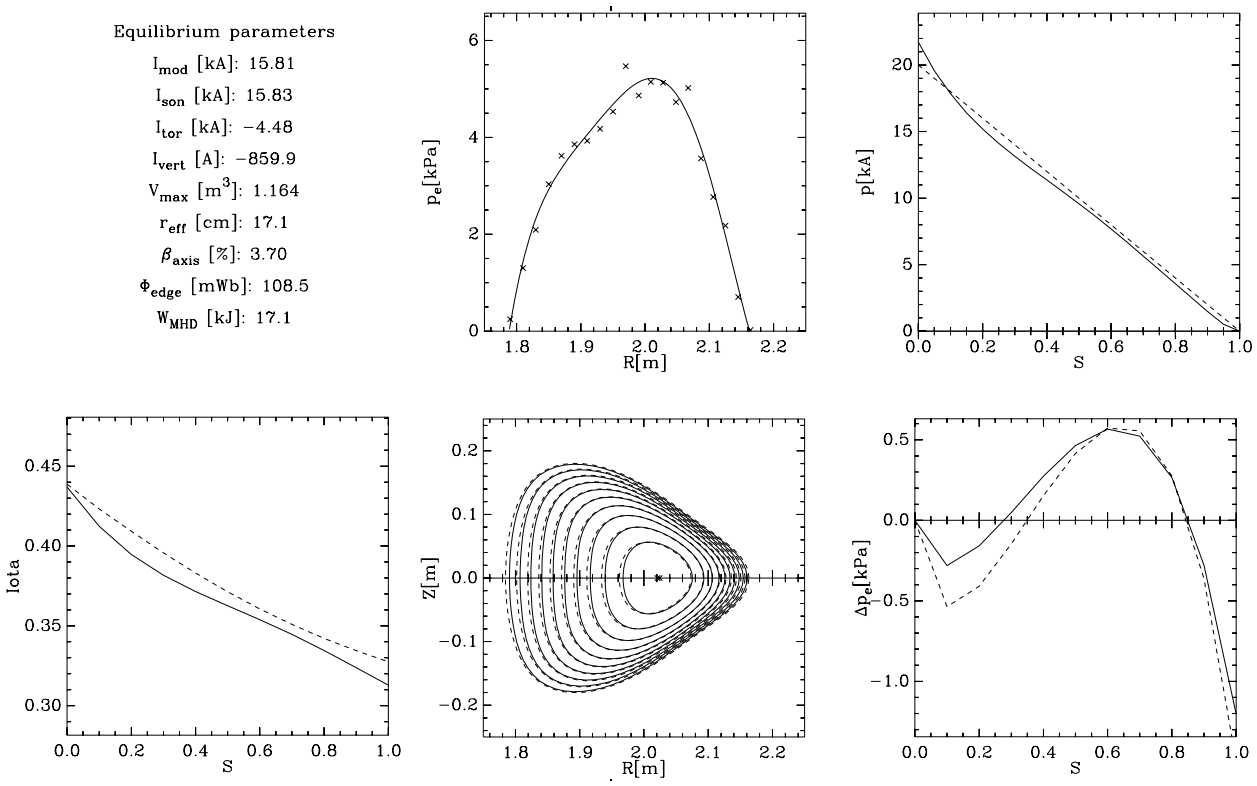

Fig. 4. Comparison of interpreted fit (solid lines) and standard NEMEC calculation (dashed) for shot #31909 (for further explanation see text).

Plasma heating in the start-up phase of LHD

Construction of LHD is proceeding on schedule, and ignition of the first plasma is scheduled at the end of March 1998. The Plasma Heating Division of the National Institute for Fusion Science (NIFS) has been undertaking technology development of heating devices for seven years. The heating schemes planned for LHD are electron cyclotron heating (ECH), neutral beam injection (NBI), and ion cyclotron resonant frequency (ICRF) heating. Certain hardware advances have been made for each of these heating schemes, but more work remains to be done to reach the final goal. Since LHD uses superconducting coils to facilitate steady-state operation of the device, emphasis was put on steady-state plasma heating. With the first experiment scheduled in the very near term, start-up of plasma heating in LHD in the initial phase is planned as shown in Table 1.

The following is a brief summary of the development work conducted by the Plasma Heating Division to support the program of Table 1.

Table 1.

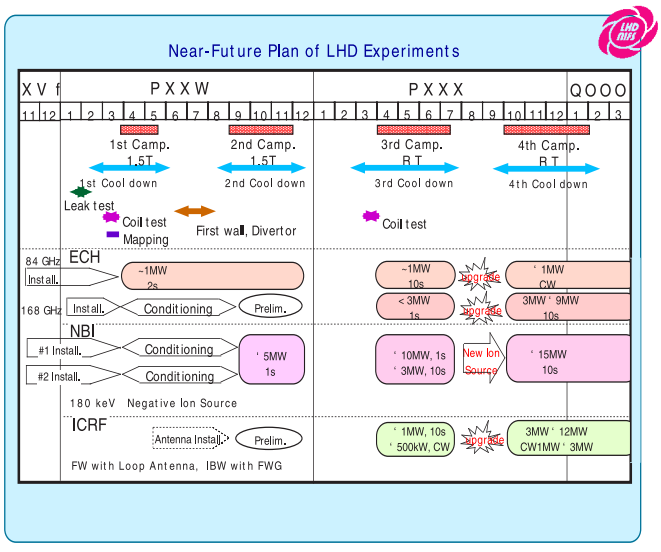

ECH

The ECH group at NIFS has developed gyrotrons at two frequencies: 84 GHz and 168 GHz. The 84-GHz gyrotron, developed in collaboration with CPI, has achieved the following operational parameters: 500 kW for2 s, 400 kW for 10 s, and 100 kW in steady-state operation. Development of the 168-GHz gyrotrons is conducted in association with JAERI and Toshiba. The 168-GHz gyrotron of NIFS can be operated at a power level of 400 kW for 100 ms. It has a relatively low efficiency $\eta \sim 20\%$, however, and further investigation must be continued to improve this.

Windows development was another important issue. NIFS proposed a Si-N window, which has been installed in one of the 168-GHz gyrotrons and tested at high power. In the initial phase of the LHD experiment, two 84-GHz gyrotrons will be used for second harmonic heating. As a backup, a Gycom gyrotron (82.7 GHz) was purchased. In addition, two 168-GHz gyrotrons will be operated in the fourth harmonic regime, though their development is not fully complete. In order to transmit ECH power from these gyrotrons, four transmission lines are under construction, as are four quasi-optical wave launchers. They will be installed by the end of December 1997.

ICRF

ICRF heating will start during the second experimental campaign, which begins in August 1998. In this initial phase, two kinds of antennas will be used: a water-cooled loop antenna which excites the fast wave from the high-field side and a folded wave guide antenna designed for slow wave excitation from the low-field side. Power at 1.6 MW for 1 h was achieved at 50 MHz from the high-power rf generator. Currently, efforts are being made to stretch the available frequency range of the generator in steady-state operation. As noted, the loop antenna is water cooled, other rf components are also designed for steady state. The most difficult components have been the feed-through and liquid-stub tuner. They have been tested in steady-state operation at 40 kV, which enables injection of 1 to 3 Mw per antenna depending on the loading resistance of the plasma. The design of the ICRF system was based on an acquired technology database and two actual antenna have been fabricated by an industrial company.

NBI

Negative-ion-based NBI was adopted for LHD plasma heating. LHD has a 4-m major radius and the best injection from the particle orbit point of view is parallel injection. The injection energy that optimizes the power deposition profile was determined to be 180 keV. Negative-ion-based NBI was a new challenge, and the development of negative ion sources was a most difficult issue, owing to the lack of knowledge in this area. Beginning in 1992, the development of a negative ion source proceeded in steps using 1/6-scale, 1/3-scale, and full-size scale model ion sources. In 1995, 16.2 A of current was extracted by using the 1/3-scale model ion source, encouraging the following developmental work. Subsequently, the beam was accelerated up to 125 keV, arc efficiency was improved up to 0.1 A/kW, beam divergence was improved up to 5–9 mrad, acceleration efficiency, $I_{H^-}/(I_{H^-} + I_e)$, reached 85%, and theoretically expected neutralization efficiency, ~60%, was achieved. The remaining objective is further improvement of acceleration efficiency to enable long-pulse operations.

Since early 1997, testing of a full-size model ion source, i.e., the one to be used after the development is completed, has been underway. The maximum current obtained so far is 20 A, with a goal of 40. Since the size of the ion source has increased, the main problem at present is nonuniformity of the plasma in the ion source.

Two beam lines are under construction with two ion sources for each beam line. Given the present status of negative ion source development, injection of 5 MW during in the second campaign should be achievable. Our final goal of 40 A will be obtained through continued development.

T. Watari, for the Plasma Heating Division
National Institute for Fusion Science
Toki, Japan

Summary of the 11th International Stellarator Conference and the 8th International Toki Conference on Plasma Physics and Controlled Nuclear Fusion

The International Stellarator Conference (under the aegis of the Stellarator Cooperation Agreement of the International Energy Agency is held every two years. The International Toki Conference on Plasma Physics and Controlled Nuclear Fusion has been held annually at Toki-city, Japan, featuring a selected topic in plasma physics and fusion engineering. This year these two conferences were held as a joint conference in Toki-city from September 29 to October 3, 1997, hosted by the National Institute for Fusion Science (NIFS) and supported by the Ministry of Education, Gifu-prefecture, Toki-city, and the Japan Society of Plasma Science and Nuclear Fusion Research. The main theme was helical system research.

There were 43 oral presentations and 101 poster presentations at the conference. The total number of participants was 211 (see Fig. 1): 132 from Japan and 79 from 12 other countries including the United States, Germany, Spain, Russia, Ukraine, China, Australia, and India. Papers presented at the conference will be published in the *Journal of Plasma and Fusion Research*. A feature of the conference was a technical tour of the superconducting Large Helical Device (LHD) nearing completion at NIFS (Fig. 2). Approximately 200 citizens attended two lectures related to fusion, an indication of the general interest in and support for fusion research in Japan. The next International Stellarator Conference will be held in 1999 in the United States.

This conference covered

- confinement-related experiments and relevant theories
- L-mode, H-mode, high-T_i mode, and the effects of radial electric fields
- new devices, advanced helical concepts, reactor studies
- steady-state operation
- physics and technology related to particle and energy balance

T. Stix gave a plenary lecture, "Highlights in Early Stellarator Research," which served as the Memorial Address for the late Prof. L. Spitzer. Keynote lectures were given by A. Iiyoshi on "Physics of Helical Confinement Systems" and by R. J. Goldston on "Implications of Recent Tokamak Research for Other Approaches to Toroidal Confinement."

Experiments

The most encouraging result was reported by the W7-AS group (Germany). In high-power NBI /ECH discharges, they achieved a confinement improvement factor of at least 2 compared to the ISS95 scaling with $T_e > T_i \sim 1.5$ keV at $n_e \sim 10^{20}$ m^{-3}. A factor of 1.2–1.4 is usually obtained in various confinement improvement modes in Heliotron-E (Japan) and the Compact Helical Device (CHS, Japan). An improvement factor of two or more is necessary for a practical reactor. Very low recycling was achieved using substantial wall conditioning in W7-AS. This resulted in a peaked density profile, which caused a steep temperature gradient and a large negative electric field close to the plasma edge. The edge density remained surprisingly constant even when both the central density and the heating power were increased. The observed electric field is consistent with that obtained from the ambipolarity condition of the neoclassical fluxes. The transport of ions and electrons is consistent with neoclassical predictions in the core region, while that in the plasma periphery is anomalous.

The electric field and its influence on transport were studied intensively in low-density ECH discharges in W7-AS. A strongly positive electric field E_r was observed, where the electron temperature profile was highly peaked with T_e (0) up to 4 keV. The value for χ_e was much lower than that obtained neoclassically assuming $E_r = 0$. The electron root feature ($E_r > 0$) was confirmed by experiments with 140-GHz ECH (second harmonic X-mode heating) where $T_e >> T_i$. It was concluded that the electric field was formed by a loss of high-energy electrons by ∇B drift instead by thermal particles. An electron root was not observed with 70-GHz ECH (fundamental mode). It was also confirmed that it is easy to enter the electron root with high ECH power, and also with large toroidal ripple. On the other hand, the electric field was determined by thermal particles for an ion root ($E_r < 0$) where $T_i \sim T_e$.

In Heliotron E (Japan), profile effects on transport were systematically studied. Values of $n_e(0)/\langle n_e\rangle = 1.2$–$4.5$, $T_i(0)/\langle T_i\rangle = 1.4$–$2.7$, and $T_e(0)/\langle T_e\rangle = 1.3$–$4.1$ were obtained with ECH and NBI (here the angle bracket indicates the volume averaged value). A peaked electron temperature profile was obtained by ECH. In this case, the density profile was always flat as universally seen in helical systems. On the other hand, researchers found peaked ion temperature profiles accompanied by peaked density profiles and improved confinement ("high-T_i mode"). However, the degree of the confinement improvement was modest, in contrast to W7-AS.

Fig. 1. Attendees of ISC-11 and ITC-8 at Ceratopia Hall, Toki-city, Japan, on September 30, 1997.

In CHS, plasma parameters were extended for both ECH and NBI plasmas. For ECH with an additional 106-GHz gyrotron, researchers achieved $T_e(0) = 2$ keV at $\langle n_e \rangle = 10^{19}$ m^{-3}, and $T_e(0) = 1$ keV at $\langle n_e \rangle = 3.5 \times 10^{19}$ m^{-3}. For NBI at 1.6 MW, they achieved $T_i(0) = 0.8$ keV at $\langle n_e \rangle = 1.5 \times 10^{19}$ m^{-3}. In this case, the density profile is peaked, and a "high-T_i mode" with confinement improvement was observed. However, the degree of confinement improvement is modest, only up to 20%. Heavy ion beam probe (HIBP) measurements of potential profiles and potential fluctuations have begun for a systematic study of the relation between electric field and transport; CHS has the most complete set of diagnostics for this purpose at present. Steady-state electric pulsation was discovered, which shows a typical example of the nonlinear relation between the radial current and the radial electric field.

Local island divertor (LID) experiments had been reported from CHS previously, but the improvement of energy confinement by the LID (~20%) was analyzed in more detail, and the evaluation of the exhaust efficiency with a fast ion gauge and a study of the behavior of the particles using a Langmuir probe array were reported.

In L-2M (Russia), the initial stage of the ECH discharge was studied. The delay of breakdown time was studied as a function of the central magnetic field strength and also with magnetic axis shift. The minimum breakdown time was about 1.5 ms when the resonance condition was satisfied at the vacuum magnetic axis ($B = 1.32$ T and $f = 75$ GHz, $P = 0.4$ MW).

In the Uragan-3M $\ell = 3$ torsatron (Ukraine), rf plasma discharge cleaning was studied, and researchers claimed that the method provided efficient removal of light impurities and reduction of neutral hydrogen recycling.

In the H-1 heliac (Australia), confinement transitions at low magnetic field ($B < 0.2$ T), low temperature ($T_i < 100$ eV), and low heating power (~50 kW) were observed. Researchers observed features similar to L-H transitions, such as steepening of the density gradient, increase of the radial electric field, suppression of turbulence, and increase of ion energies. Next year H-1 will move to higher B fields (1 T) and higher heating power (200 kW).

Researchers from TJ-II (Spain), completed in December, 1996 gave the results of magnetic surface measurements. Measurements were performed by injection of an electron beam of 100–200 eV at $B = 500$ G with a fluorescence method. Observations in each magnetic field configuration agree well with the calculated values, and high accuracy of the coil and vacuum chamber installation was demonstrated. The TJ-II group is about to start 1-MW, 53.2-GHz ECH experiments.

New devices under construction

A quasi-helically symmetric (QHS) stellarator, the Helically Symmetric Experiment (HSX), is under construction at the University of Wisconsin (USA); it will be completed in early 1998.

LHD (NIFS, Japan) is the world's largest helical system. The superconducting helical and poloidal coils of LHD have been completed and the vacuum containers are being processed. It was clearly shown that LHD construction has reached the final phase. After careful commissioning of the vacuum and coil cooling systems, and production of a magnetic field by the superconducting coils, ECH experiments

at B = 1.5 T will start at the end of March 1998. Many presentations were made on LHD experimental plans such as confinement, stability, steady-state operation, divertor, and so on.

Construction of the W7X helias (Germany) has started, aiming at completion in 2005. Physics issues such as divertor operation, influence of the beta value on the magnetic islands for each magnetic field configuration, and MHD characteristics were examined.

As a successor to Heliotron E, a project to construct an ℓ = 1 helical-axis configuration is underway at Kyoto University (Japan) with completion expected in 1999. The Kyoto group expect reduced neoclassical transport and a higher beta value with small bootstrap current.

New configurations

The small-aspect-ratio toroidal hybrid (SMARTH) study (USA) was developed using the concept of bounce-averaged omnigeneity. A small aspect ratio of ~3 can be achieved, and calculations show that it is stable to ballooning modes for volume averaged beta of 6%.

Devices with magnetic fields that are nearly toroidally symmetric in Boozer coordinates have been studies extensively. The group at Princeton (USA) studied the design of devices of the MHH2 type, originally proposed by P. Garabedian. They were considering the possibility of utilizing modular coils, a conducting shell, and saddle coils, along with usage of some existing facilities. Also based on the same MHH2 concept, the Quasi-toroidal Stellarator (QUATOS) was designed by the group at Auburn University (USA).

A quasi-axisymmetric stellarator with aspect ratio of 4.2 was proposed by a group at NIFS. It has a tokamak-like axisymmetric magnetic field structure and very small helical ripple. Thus, large velocity shear is expected to reduce anomalous transport.

Some reactor studies were also presented, and these indicate the necessity of confinement improvement by about a factor of two from the present levels.

Theory

Various configurations were proposed for configuration optimization. These include quasiaxisymmetric systems, quasihelical symmetric systems, and quasiomnigeneous or quasi-isodynamic systems. Especially, quasiaxisymmetric systems were extensively examined in relation to the proposal of new devices. Typical properties of those systems are low aspect ratio, a small number of toroidal field periods, and active use of the bootstrap current in order to obtain a high equilibrium and stability beta limit. In the sense that the net toroidal current is actively utilized, these systems represent a new concept for helical systems, and thus profile control of both the pressure and net toroidal current is quite important. The HINT and PIES codes, which allow magnetic islands, are being modified in order to calculate such equilibria including the net toroidal current such as bootstrap current, Ohkawa current, and Ohmic current. Ballooning modes are being intensively studied and were discussed actively during the meeting. Using high-mode-number analysis, their destabilizing mechanism in the region with stellarator-like high magnetic shear was clarified, and the existence of both tokamak-like modes and modes inherent to 3-D equilibria was shown in an LHD-like heliotron/torsatron system.

The properties and the dangers of ballooning modes with finite mode number were being examined by using a 3-D stability code, CAS3D. The ballooning modes inherent to 3-D equilibria were considered to have quite high poloidal and toroidal mode numbers that they localize in the both poloidal and toroidal directions; they may be stabilized by finite Larmor radius effects.

A Monte Carlo simulation code in 5-D phase space was developed based on a technique similar to the adjoint equation for dynamic linearized problems. Such a Monte Carlo code was applied to W7-AS experiments with ECRH to estimate the kinetic effects of suprathermal electrons. The important role of the radial diffusion of suprathermal electrons in the broadening of the ECRH deposition profile was clarified. Clarification of anomalous transport mechanisms remains unresolved as in tokamaks, although substantial theoretical and experimental efforts have continued. However, the important role of the radial electric field in transport phenomena and improved confinement has been recognized. Many numerical tools for MHD equilibrium and stability, and particle orbit and heating are becoming mature, leading to a deeper understanding of experimental results.

Masami Fujiwara, Shigeru Sudo, Keisuke Matsuoka, and Noriyoshi Nakajima